Atmos. Chem. Phys. Discuss., 10, 11109–11138, 2010
www.atmos-chem-phys-discuss.net/10/11109/2010/
© Author(s) 2010. This work is distributed under
the Creative Commons Attribution 3.0 License.

Atmospheric Chemistry and Physics Discussions

This discussion paper is/has been under review for the journal Atmospheric Chemistry and Physics (ACP). Please refer to the corresponding final paper in ACP if available.

# Optical extinction by upper tropospheric/stratospheric aerosols and clouds: GOMOS observations for the period 2002–2008

**F. Vanhellemont[1], D. Fussen[1], N. Mateshvili[1], C. Tétard[1], C. Bingen[1], E. Dekemper[1], N. Loodts[1], E. Kyrölä[2], V. Sofieva[2], J. Tamminen[2], A. Hauchecorne[3], J.-L. Bertaux[3], F. Dalaudier[3], L. Blanot[3,4], O. Fanton d'Andon[4], G. Barrot[4], M. Guirlet[4], T. Fehr[5], and L. Saavedra[5]**

[1]Belgian Institute for Space Aeronomy, Brussels, Belgium
[2]Finnish Meteorological Institute, Helsinki, Finland
[3]Service d'Aéronomie du CNRS, Verrieres-le-Buisson, France
[4]ACRI-ST, Sophia-Antipolis, France
[5]ESA-ESRIN, Frascati, Italy

Received: 26 January 2010 – Accepted: 20 April 2010 – Published: 26 April 2010

Correspondence to: F. Vanhellemont (filip.vanhellemont@aeronomie.be)

Published by Copernicus Publications on behalf of the European Geosciences Union.

## Abstract

Although the retrieval of aerosol extinction coefficients from satellite remote measurements is notoriously difficult (in comparison with gaseous species) due to the lack of typical spectral signatures, important information can be obtained. In this paper we present an overview of the current operational nighttime UV/Vis aerosol extinction profile results for the GOMOS star occultation instrument, spanning the period from August 2002 to May 2008. Some problems still remain, such as the ones associated with incomplete scintillation correction and the aerosol spectral law implementation, but good quality extinction values can be expected at a wavelength of 500 nm. Typical phenomena associated with atmospheric particulate matter in the Upper Troposphere/Lower Stratosphere (UTLS) are easily identified: Polar Stratospheric Clouds, tropical subvisual cirrus clouds, background stratospheric aerosols, and post-eruption volcanic aerosols (with their subsequent dispersion around the globe). In this overview paper we will give a summary of the current results.

## 1 Introduction

Upper tropospheric and stratospheric particles (whether liquid or solid) are intensively studied for a number of reasons that can be roughly summarized as follows: (1) they have an impact on the Earth radiative balance due to their optical properties, (2) they play a crucial role in heterogeneous chemistry, and (3) they provide information on the emission of precursor species from which they originate. Here, the word 'particles' should be taken in its most general context: liquid or solid aerosols of submicron size, cloud droplets or crystals with sizes of tens or hundreds of microns, etc. From previous experiences with satellite occultation instruments, we know that a few particle types are commonly encountered in the measurements: stratospheric aerosols, tropical subvisual cirrus clouds and Polar Stratospheric Clouds (PSCs).

The stratospheric aerosol layer (or Junge layer, named after its discoverer; see



ACPD

10, 11109–11138, 2010

Junge et al., 1961) consists of liquid droplets composed of a mixture of sulphuric acid and water. The layer manifests itself in a pronounced way after major volcanic eruptions that are powerful enough to inject teragrams of $SO_2$ into the stratosphere, such as the ones of Mount Pinatubo (the Philippines, 1991) or El Chichón (Mexico, 1982); see Robock (2000). After an oxidation process, sulfate aerosols are formed that are subsequently transported globally, depending on the latitude of the eruption. Eventually they are removed from the stratosphere, although this process can take years. Nevertheless, the last major eruption (Mount Pinatubo) dates already from 18 years ago, and the stratospheric aerosol layer returned to its "background" level around 1997. Since then, no significant trend is observed in data from SAGE II, balloon-borne instruments and lidars (Deshler et al., 2003, 2006), even when compared with volcanically quiet years such as 1979. These findings suggest a more or less stable input of sulphuric species in the stratosphere that maintain the background layer. Crutzen (1976) suggested carbonyl sulfide (OCS) as the major precursor gas, although this hypothesis has been challenged (see e.g. Chin and Davis, 1995; Leung et al., 2002). Very recently, increased anthropogenic $SO_2$ emission by coal burning in China has been proposed as a possible origin for an upward trend in lidar measurements of stratospheric aerosols (Hofmann et al., 2009).

Polar Stratospheric Clouds have been investigated for over two decades now. The well-known classification scheme of PSCs was originally based on observations of backscatter and depolarization ratios with lidar instruments (Poole and McCormick, 1988). Type Ia particles are believed to be relatively large crystalline particles consisting of hydrates of $HNO_3$ such as Nitric Acid Trihydrate (NAT) or Dihydrate (NAD). The smaller, liquid Type Ib particles consist of a supercooled ternary solution (STS) of $HNO_3$, $H_2SO_4$ and $H_2O$. The crystalline Type II particles are formed of pure water ice. PSCs have a crucial role in the stratospheric ozone depletion process over the Arctic and Antarctic regions, because of (1) heterogeneous chemistry on the particle surface and (2) the denitrification of the atmosphere by the sedimentation of mainly Type Ia particles. Formation of PSCs is driven by temperature: Type Ia and Ib particles form



ACPD
10, 11109–11138, 2010

below about 195 K, while the Type II ice crystals form at the ice frost point, about 188 to 190 K in the lower stratosphere. These cold temperatures are provided in the polar regions during local winter.

The so-called subvisual cirrus clouds are a fairly recent discovery for the obvious reason that they are optically thin and thus invisible from the ground (hence the name): an upper limit for the optical thickness of 0.03 at 694 nm is sometimes mentioned in the literature. Long optical pathlengths ensure that satellite occultation instruments such as SAGE II have detected them frequently (Wang et al., 1996). They are mainly found in the tropics and midlatitudes, around the tropopause altitude region (16–17 km). Much is still to be learned about the formation of these clouds, but Jensen et al. (1996) proposed at least two mechanisms: (1) they originate from horizontal anvil-shaped outflows of large convective cumulonimbus clouds, and (2) from nucleation inside a humid layer that experiences slow uplift through the extremely cold region of the tropopause. Subvisual cirrus form cloud layers with a very large horizontal extent (hundreds of kilometers) but are at the same time very thin (smaller than 1 km). In recent years they received a lot of attention due to their possible role in the radiative balance of the atmosphere, their impact on ozone concentrations through heterogeneous chemistry (Solomon et al., 1997), and their role in the dehydration of air that enters the tropical lower stratosphere (Jensen et al., 1996).

The Global Ozone Monitoring by Occultation of Stars (GOMOS) instrument was primarily intended to deliver accurate altitude profiles of trace gas concentrations. These retrievals can be performed since each gas is detected by its specific spectral signature in the measured light intensity. Atmospheric particle populations pose a more challenging problem since the spectral shape is unknown, with the direct consequence that it is a priori impossible to find out which kind of particles are in the line of sight of the instrument. This is the reason why GOMOS delivers only one common product, perhaps somewhat misleadingly dubbed “aerosol extinction”. It should be understood that this data product currently embraces all above-mentioned types of aerosol and cloud particles (or indeed even any unknown extinction phenomenon with a smooth



ACPD
10, 11109–11138, 2010

spectral dependence). However, the distinction will be made in this paper with the use of additional information, such as time of appearance/disappearance, geolocation and altitude.

First results on GOMOS aerosol/cloud extinction profiles representing the year 2003 were previously published (Vanhellemont et al., 2005). This paper presents results for the period 2002–2008.

## 2 GOMOS: instrument and obtained data set

The GOMOS instrument has been adequately described elsewhere (Kyrölä et al., 2004; Bertaux et al., 1991, 2000, 2010), so we only give a brief summary here. GOMOS, onboard ENVISAT, was launched in a sunsynchroneous orbit on 1 March 2002. GOMOS routine operations started in August 2002, and since then the instrument has been recording data almost continuously until present. GOMOS observes occultations of stars (chosen from a predefined catalogue) behind the earth limb, and records the received light intensity in the UV/Vis/NIR spectral range: 248–690 nm (spectrometers A1 and A2), 755–774 nm (spectrometer B1) and 926–954 nm (spectrometer B2). From measured signals, transmittances are calculated that in turn are used to derive altitude concentration profiles for $O_3$, $NO_2$, $NO_3$, $H_2O$ and $O_2$, and temperature profiles. Furthermore, aerosol/cloud extinction profiles at different wavelengths are obtained.

It is important to know that the uncertainty on the obtained profiles is largely determined by the magnitude and temperature of the observed star. But even bright stars (such as Sirius) are weak light sources in comparison with the Sun; profiles obtained from stellar occultations have therefore larger uncertainties than the ones from solar occultations. This disadvantage is however largely compensated for by the fact that stars are abundant in the sky: about 30 to 40 occultations have been typically observed per orbit, although this number decreased to 20 or 30 occultations per orbit after an instrument malfunction in 2005. Hundreds of thousands of occultations have been observed by GOMOS since the start of the mission.



ACPD
10, 11109–11138, 2010

The occultation statistics for the period August 2002–May 2008 (a total of about 600 000 events, the entire data set that was available to us at the time of writing) are represented by histograms in Fig. 1. Of course, the lower number of occultations for the years 2002 and 2008 are caused by an incomplete sampling of these years, while the smaller number in 2005 resulted from the instrument failure mentioned earlier. Longitudinal sampling is clearly very homogeneous. Most occultations occur at midlatitudes, although plenty of polar measurements are available. Most stars have moderate to weak brightness, and are rather cold. Also, about half of the occultations occur in the Sun-illuminated atmosphere ("bright limb", Solar Zenith Angle SZA<100), the other half in "dark limb" (SZA≥100). More details about the solar illumination condition and its consequences are given below.

## 3 Retrieval method

### 3.1 Spectral behaviour

As already said above, the particle optical extinction spectrum is a priori unknown. Therefore, the actual optical spectrum is treated as a product of the retrieval algorithm. It is far from clear how such a particle optical spectrum should be parameterized, but we can be guided by the fact that usual atmospheric particle size distributions are broad, covering a few orders of magnitude, and the resulting optical spectra are thus smooth. Hence they are often described with analytic, smooth functions, such as polynomials. For data version 6.0, the GOMOS Science team chose to implement a quadratic polynomial as a function of wavelength for the simple reason that it is versatile: large (constant spectrum), medium-sized (peak at mid-visible wavelengths) or small particle spectra ($\beta \sim \lambda^{-4}$) can within good approximation be captured by such polynomials. Retrieval algorithms for other satellite occultation instruments are often also equipped with this feature. Furthermore, Vanhellemont et al. (2006) showed with simulated data (using a Mie code) that a quadratic polynomial is a good choice when one wants to



ACPD
10, 11109–11138, 2010

obtain good aerosol retrievals without introducing too many degrees of freedom in the retrieval problem.

### 3.2 Spectral/spatial inversion

The GOMOS retrieval algorithm has been described in detail in another paper of this special issue (Kyrölä et al., 2010). Here it suffices to say that the retrieval consists of two parts: (1) the spectral inversion, where measured transmittance spectra at each tangent altitude separately are inverted to slant path integrated column densities (for gases) and optical thickness (for particles), and (2) the spatial or vertical inversion, where the retrievals of the first step are separately inverted to local concentration profiles (gases) and optical extinction profiles (particles). This second step is performed in combination with a Tikhonov altitude smoothing (Twomey, 1985; Rodgers, 2000) in order to get partially rid of the perturbations caused by residual scintillation in measurements taken during very inclined occultations (Sofieva et al., 2009). The amount of smoothing is determined by a predetermined target resolution for the profile. For particles, a profile resolution of 4 km was chosen since unsmoothed profiles showed strong oscillations; aerosol extinction spectra have the tendency to swallow a large portion of the residual scintillation perturbations. Nevertheless, fine-scale structures (e.g. thin clouds) are smeared out due to this feature.

It is in the spectral inversion model that the slant path particle optical thickness is implemented as a quadratic polynomial:

$$\tau(\lambda) = \sigma_{\text{ref}}(r_0 + r_1 \Delta\lambda + r_2 \Delta\lambda^2)$$

with $\Delta\lambda = \lambda - \lambda_{\text{ref}}$ and $\lambda_{\text{ref}} = 500\,\text{nm}$ a reference wavelength. For scaling purposes, a "cross section" $\sigma_{\text{ref}} = 6 \cdot 10^{-10}\,\text{cm}^2$ was used. Notice that only the first parameter $r_0$ has a direct physical meaning: $\sigma_{\text{ref}} r_0$ equals the particle slant path optical thickness at 500 nm. During the spatial inversion, this parameter receives Tikhonov-style altitude smoothing, while the other parameters remain unconstrained. Retrospectively, this



ACPD
10, 11109–11138, 2010

turned out to be a poor methodology: while the obtained extinction profiles at 500 nm look quite good, the spectra at other wavelengths are often very noisy.

Finally, it should be mentioned that during the spectral inversion, the optical extinction spectra from the neutral air (Rayleigh scattering) are removed instead of retrieved from the measurements, using external ECMWF (European Centre for Medium-range Weather Forecasts) air density data, to avoid interferences with the residual scintillation and the spectrally similar aerosol contribution. Also, only spectrometer A measurements are currently used for the aerosol retrieval.

### 3.3 The homogeneous layer assumption

Occultation measurements have a limited information content. Hence the assumption of homogeneous atmospheric layers that is so often found in retrieval codes: the number of unknowns is drastically reduced, leading to a more stable inversion. For more or less uniformly mixed gases and particles (such as stratospheric aerosols), the assumption should hold quite well. However, when local phenomena (such as clouds) are observed, the assumption is wrong: the phenomenon affects the light ray only locally. This should be taken into account whenever we analyse retrievals of PSCs and volcanic plumes, for example: the obtained extinction coefficients should be seen as slant path equivalent values.

### 3.4 Bright limb versus dark limb retrievals

When the optical light path traverses the Sun-illuminated atmosphere, parts of the atmosphere located in the field-of-view scatter additional light into the instrument, which means that the simple optical transmission model for the retrieval is not correct anymore. This was anticipated: the additionnal upper and lower CCD bands in GOMOS were implemented to correct for this background illumination (Bertaux et al., 2010; Kyrölä et al., 2010). However, post-launch processing showed that the correction is not perfect. The situation is particularly bad for the aerosol extinction profiles, since their




CC BY

smooth optical extinction spectrum strongly resembles the limb signal. The aerosol extinction retrievals typically show unrealistic features at very high stratospheric altitudes. At present, the best we can do is exclude the bright limb profiles from data analysis. Investigations showed that occultation events with a solar zenith angle of 100° or larger deliver unperturbed, dark limb aerosol retrievals.

### 3.5 Retrieval results

In summary, the GOMOS particle extinction profiles have acceptable quality around 500 nm, but are oversmoothed. At other wavelenghts, the profile quality is poor, and we therefore exclude them from further study. Furthermore, it is best to exclude the aerosol profiles in bright limb (SZA<100): from the entire data set of 600 000 occultations, about 301 000 remain to be exploited. Among these, some are still perturbed by residual scintillation. These perturbations are visible in individual aerosol extinction profiles. When averaging large numbers of profiles (see e.g. the zonal plots below), the perturbations disappear, confirming that they are random in nature, with zero mean.

Like all profiles derived from occultation measurements, GOMOS aerosol extinction profiles are increasingly more uncertain when we descend to lower altitudes, because the transmitted light intensity becomes weaker. In principle, a cut-off altitude can be defined, below which no aerosol information is present anymore. This altitude depends on the wavelength considered, and the magnitude and temperature of the star, and therefore changes from one occultation to the next. At 500 nm, an average limit of 10 km can be considered as the value below which the profiles are not trustworthy anymore.

On Fig. 2, we present individual GOMOS extinction retrievals at 500 nm for a number of particle types. It is impossible to distinguish these types using only one wavelength; the presented profiles were selected after analysis of the entire GOMOS data set and knowledge about geolocation and time of occurence of these particle phenomena (see further on in this paper).

It is clear that the profiles are oversmoothed. For instance, tropical subvisual clouds

are known to be horizontally extended cloud layers that are quite thin, having a thickness smaller than 1 km (Jensen et al., 1996); the example on the figure clearly shows that the layer has been spread out by the smoothing constraint.

## 4 Comparisons with other instruments

A detailed validation study for the GOMOS aerosol extinction profiles has not been performed yet. Nevertheless, Vanhellemont et al. (2008) already performed comparisons with the results derived from the imagers of the Atmospheric Chemistry Experiment ACE (Bernath et al., 2005). Here, we present first comparisons with aerosol extinction profiles from the Stratospheric Aerosol and Gas Experiment II (SAGE II; see Chu et al., 1989), its follow-up SAGE III (Thomason and Taha, 2003) and the Polar Ozone and Aerosol Measurement POAM III (Lucke et al., 1999). As already stated, only dark limb measurements were considered. Furthermore we avoided PSCs by excluding occultations inside the polar vortex: apart from the wrong assumption of homogeneous layers, two different instruments with two different viewing geometries will deliver two different profiles for the same cloud. A coincidence window of 500 km and 1/2 day was used, allowing us to find a fairly large comparison data set, summarized in Table 1. Notice that we used a spectral channel of each instrument that is close to the GOMOS reference wavelength of 500 nm. Furthermore, GOMOS data were interpolated to these wavelengths using the retrieved quadratic polynomial.

For the $i$-th coincidence, the difference between GOMOS (GOM) and the other instrument (SAT), relative to the mean of the two, was evaluated as follows:

$$\Delta_i = 100 \times 2 \frac{(p_{\mathrm{GOM},i} - p_{\mathrm{SAT},i})}{|p_{\mathrm{GOM},i} + p_{\mathrm{SAT},i}|}$$

As statistical estimators for the entire data set, we prefered to use the median (50th percentile) since it is more robust with respect to outliers than the numerical mean. The variance of the data set was calculated with the 16th and 84th percentile. The obtained



ACPD
10, 11109–11138, 2010

statistical estimates are shown in Fig. 3. As can be seen, the comparisons are quite good at upper tropospheric/lower stratospheric altitudes. Differences with SAGE II are within 20% from 10 to 25 km, a conclusion that can also be drawn for the SAGE III comparisons. The median differences with POAM III are even smaller, within 10% from 11 to 22 km. Notice however that the variance is much larger than for the SAGE II/III comparisons.

## 5 Results

### 5.1 Yearly zonal statistics

A coarse idea about the presence of aerosols and clouds in the upper troposphere/lower stratosphere can be gained by considering zonal yearly statistics. Ranging from 90° S to 90° N, 72 latitude bins with a width of 2.5 degrees were defined. Aerosol extinction profiles were linearly interpolated on a common altitude grid ranging from 1 to 50 km with a spacing of 1 km. Yearly statistics were subsequently calculated on all data within one bin. Once again: we used percentiles as statistical estimators since extinction values are not necessarily normally distributed and because the median (50th percentile) is rather insensitive to outliers. We should also mention that yearly zonal statistics are seasonally biased when we use only dark limb measurements, since Arctic/Antarctic summer is not sampled. The median particle extinction at 500 nm is shown in Fig. 4 for every GOMOS mission year. A few phenomena are readily observed: (1) the umbrella-shaped stratospheric aerosol layer that is highest at the equator, lowest at the poles, (2) higher extinction values in the Antarctic (and to a lesser extent Arctic) stratosphere that are caused by PSCs, and (3) higher extinction values in a localized tropical zone at an altitude of about 16–17 km due to subvisual cirrus clouds. The picture is almost systematic for every year, but there are some significant differences however. First notice that Antarctic PSCs are less pronounced for the years 2002 and 2008 because the Antarctic PSC season is not well sampled in those

years: the data set starts end of August 2002 and ends in May 2008. More important, stratospheric aerosol extinction levels are much higher in 2007 and remain elevated even in 2008, suggesting the formation of new aerosols following stratospheric injection of $SO_2$ by a volcanic eruption. This is the case; the Soufrière Hills eruption (see below) in May 2006 is most likely the source. Furthermore, 2005 also seems to exhibit elevated aerosol levels, although the picture is noisier due to the incomplete sampling of the year (instrument failure).

Equally interesting is the yearly zonal variability of the 500 nm aerosol extinction values, calculated as half the difference between the 84th and 16th percentile. The variability is of course determined by the S/N-ratio of the measurements and (more importantly) by natural aerosol/cloud variability, caused by the appearing, disappearing and atmospheric transport of particles. This is clearly visible on Fig. 5. Typical "on/off-events" such as clouds (tropical cirrus, PSCs) exhibit large variability, while slowly changing features (such as the stratospheric aerosol layer) vary little within one year. Notice once again that the Antarctic PSC variability during 2002 and 2008 is weak since these years have not been completely sampled. At lower, tropospheric altitudes, we see large variability due to a combination of larger profile uncertainty (measured signals are weaker) and tropospheric clouds.

### 5.2 Volcanic stratospheric aerosols

The observed elevated extinction levels in 2005 and 2007 require a more detailed investigation. On Fig. 6, we present aerosol extinction values at an altitude of 20 km (which lies above the subvisual cirrus altitudes) for the period 2004–2006, in a tropical latitude band from 6° N to 26° N. Three distinct periods can be seen. First, we observe low background aerosol levels until the end of 2004. Second, from early 2005 to the beginning of June 2006, large data gaps are present due to instrument failure. Nevertheless, the data seem to suggest a declining tail following a volcanic eruption, especially if we take the small set of data points at early 2005 into account. And third, in early July 2006 we observe a sudden increase by about a factor of 3 in extinction




CC BY

levels. The same conclusions are drawn when inspecting the evolution in latitude and time on Fig. 7. It is clear that at least two volcanic events in the tropics should be considered.

The elevated values in 2005 are most likely caused by stratospheric sulfate aerosols, formed out of the $SO_2$ cloud injected in the stratosphere by the eruptions of the Manam volcano (Papua New Guinea, 4.080° S, 145.037° E) on 27 and 28 January (Kamei et al., 2006). Manam is one of the most active volcanoes in the region; the above mentioned eruptions followed ongoing volcanic activity that started already in October 2004. An image taken by the infrared Aqua/MODIS (Moderate Resolution Imaging Spectroradiometer) indicates that the ash clouds of the first eruption on 27 January reached to over 20 km altitude, well into the stratosphere. The ash clouds of the second eruption on 28 January ascended to 18 km altitude (Smithsonian Institution, 2005). Several days later, stratospheric aerosol layers were detected twice between about 18 to 20 km altitude (layer thickness ranging from 0.2 to 1.4 km) by a shipboard lidar using a Nd:YAG laser operated at 1064 nm and 532 nm (Kamei et al., 2006). The layers were detected in the Western Pacific around 0–2° N, 156° E (3–4 February 2005) and 7–9° N, 156° E (9–10 February). Inspecting Fig. 7, we see that the amount of injected sulfur was large enough to leave a significant aerosol trace in the GOMOS data during the largest part of 2005.

The source for the elevated aerosol levels in the second half of 2006 and 2007 has been identified as the eruption of the Soufrière Hills volcano (16.72° N, 62.18° W, Montserrat, West Indies), on 20 May 2006. Immediately following the collapse of the eastern volcano flank, an eruption column of ash and gases rose to at least 17 km. Prata et al. (2007) used a combination of satellite instruments (Aqua/AIRS, MSG/SEVIRI, MLS, OMI and CALIPSO/CALIOP) to reconstruct the event and its immediate aftermath. They found that an estimated 0.1 Tg(S) was injected in the stratosphere in the form of $SO_2$, after which the gas cloud traveled westward at an altitude of about 20 km. Carn et al. (2007) on the other hand used OMI data to obtain an estimated 0.22 Tg of $SO_2$. They also reported CALIPSO/CALIOP lidar backscatter

measurements of the associated stratospheric aerosol layer as early as 7 June 2006, at an altitude of 20 km. The layer remained visible in the CALIOP data until 6 July. However, as Thomason et al. (2007) remarked, in general the stratospheric aerosol layer remains quite invisible in CALIOP backscatter measurements, while occulation instruments such as SAGE II have no problem with the detection. No doubt this is caused by the preferential forward scattering of light by small particles, in combination with longer optical path lengths. The fact that GOMOS identifies stratospheric sulfate aerosols well after the eruption date is illustrated in Fig. 8, which shows the appearing and poleward transport of the sulfuric acid particles.

Figures 7 and 8 also indicate that it took roughly one year for the Soufrière Hills aerosol cloud to cover the entire globe. Elevated extinction levels remained present until at least the end of 2007. In the months following the Soufrière Hills eruption, a few other eruptions possibly impacted the stratospheric aerosol layer. Hofmann et al. (2009) briefly mentioned the 14 July 2006 Tungurahua eruption (Ecuador, 1.467° S, 78.442° W), less than a month after the Soufrière Hills eruption. And Thomason et al. (2007) showed CALIOP observations of the volcanic plume resulting from the 7 October 2006 Tavurvur eruption (Rabaul, Papua New Guinea, 4.271° S, 152.203° E). Both are equatorial volcanoes that possible injected sulfur into the stratosphere, hereby enhancing the already existing Soufrière Hills perturbation. From GOMOS data it is at present unclear wether or not the existing volcanic aerosol layer was replenished with new sulfate aerosols originating from these eruptions.

### 5.3 Polar Stratospheric Clouds

GOMOS observes PSCs quite well. Strongly enhanced optical extinction is measured every year in the Antarctic PSC season (roughly from the end of May to October), with values typically 3 or 4 times larger than in normal background conditions. These kind of criteria (latitude, time of year, extinction values above a certain treshold) allow us to identify the presence of a PSC. It is however temperature that is the main driver for the formation of PSCs, as can be seen on the top panel of Fig. 9. Shown are all GOMOS




CC BY

aerosol extinction measurements at 500 nm taken in 2004 at an altitude of 20 km for the latitude band from 90° S to 55° S. This data set represents a mixture of measurements inside and outside the Antarctic vortex (PSCs and stratospheric aerosols), but plotted against temperature the differentiation is very clear: clouds are formed below about 195 K, the known formation temperature of NAT and STS PSCs. It is however less clear from the data whether or not Type II PSCs form at even lower temperatures. Ideally, differentiation of different types of PSC with UV/Vis/NIR data should be done by inspecting particle size distributions, or the shape of the associated optical spectrum. Methods have already been devised in the past for the SAGE and POAM instruments to make a distinction between Type Ia and Ib particles, based on the assumption that the latter are smaller than the former, with a different extinction spectrum as a consequence (Strawa et al., 2002; Poole et al., 2003). The second panel of Fig. 9 shows the ratio of 600 nm to 400 nm GOMOS optical extinction. Theoretically, very small particles ($\beta(\lambda) \sim \lambda^{-4}$) should lead to a value of 0.2, while large particles ($\beta(\lambda) = \text{constant}$) should have a value of 1. The data are extremely noisy due to the already mentioned problem with the aerosol spectral law implementation. Nevertheless, the data cloud is more or less situated between the theoretical limits, and larger particles are observed below 195 K, as expected. The data show also that it is currently impossible to differentiate between different PSC types.

## 6 Conclusions

The current GOMOS operational aerosol/cloud product consists of optical extinction profiles at 500 nm and additional spectral coefficients to evaluate the extinction at other wavelengths as well. The quality of the product is not optimal yet, due to a problematic spectral law implementation, combined with an altitude smoothing that is too strong. Furthermore, profiles derived from bright limb measurements are currently not usable. Nevertheless, if we restrict ourselves to the use of 500 nm extinction profiles retrieved from dark limb measurements, then the quality can be considered as good, although




CC BY

fine structure (thin cirrus clouds, cloud inhomogeneities etc.) has been smoothed. A comparison with SAGE II, SAGE III and POAM III showed good agreement within 20% in the upper troposphere/lower stratosphere, from 10 km to about 25 km.

All the atmospheric particle types that are expected to be observed by a satellite occultation instrument have been detected by GOMOS: the background stratospheric sulfate aerosol layer (or Junge layer) with its typical umbrella-shaped form, sulfate aerosols from volcanic origin, tropical subvisual cirrus clouds just below the tropopause at an altitude of about 16–17 km, and PSCs in the polar regions. The cloud-type events (PSCs and cirrus) have a strong yearly variability, while the Junge layer remains remarkably constant within one year.

The last major volcanic $SO_2$ injection into the stratosphere dates already from almost 18 years ago (Mount Pinatubo, 1991), with the consequence that current aerosol levels are extremely low. So low that the effect of "moderate" volcanic eruptions becomes visible in the GOMOS aerosol record. One might wonder if the so-called background is not only maintained by the typically mentioned sources (OCS, recently even anthropogenic sulfate from coal burning in China), but as well by these moderate volcanic eruptions, that are much weaker than the catastrophic events (Mt. Pinatubo, Mt. St. Helens, El Chichón), but much more frequent. In the GOMOS data, the aerosol enhancements resulting from the eruptions of Manam (Papua New Guinea) and Soufrière Hills (Montserrat, West Indies) have been identified. In the latter case, GOMOS was clearly able to track the global dispersion of the aerosols. In the aftermath of the eruption, two other possible intrusions should in principle be visible: Tungurahua (Ecuador) and Tavurvur (Papua New Guinea). We hope to identify them in future aerosol profile improvements.

The dynamics of PSCs have been studied previously with GOMOS data (Vanhellemont et al., 2005). Here, the theoretical PSC temperature dependence was clearly confirmed by GOMOS observations. The data show also roughly that particle size information is present in the GOMOS data. This is an important conclusion for future studies on the microphysics of PSCs.



ACPD
10, 11109–11138, 2010

As of February 2009, our team has been involved in a new project (AERGOM, an ESA financed project) to develop an improved algorithm that should deliver significantly better aerosol extinction profiles (at all GOMOS wavelengths) in the close future. A cloud-Type Identification method will also be devised. This will enable us to derive particle size distributions, and to study the microphysics of the observed particle phenomena.

*Acknowledgements.* This work came into existence with the financial aid of the Belgian Federal Science Policy Office (BELSPO) and the European Space Agency (ESA) through the AERGOM project (Contract No. 22022/08/I-OL). ENVISAT is an ESA mission andGOMOS is an EFI (ESA Funded Instrument).

## References

Bernath, P. F., McElroy, C. T., Abrams, M. C., Boone, C. D., Butler, M., Camy-Peyret, C., Carleer, M., Clerbaux, C., Coheur, P.-F., Colin, R., DeCola, P., DeMazière, M., Drummond, J. R., Dufour, D., Evans, W. F. J., Fast, H., Fussen, D., Gilbert, K., Jennings, D. E., Llewellyn, E. J., Lowe, R. P., Mahieu, E., McConell, J. C., McHugh, M., McLeod, S. D., Michaud, R., Midwinter, C., Nassar, R., Nichitiu, F., Nowlan, C., Rinsland, C. P., Rochon, Y. J., Rowlands, N., Semeniuk, K., Simon, P., Skelton, R., Sloan, J. J., Soucy, M. A., Strong, K., Tremblay, P., Turnbull, D., Walker, K. A., Walkty, I., Wardle, D. A., Wehrle, V., Zander, R., and Zou, J.: Atmospheric Chemistry Experiment (ACE): Mission overview, Geophys. Res. Lett., 32, L15S01, doi:10.1029/2005GL022386, 2005. 11118

Bertaux, J., Kyrölä, E., and Wehr, T.: Stellar occultation technique for atmospheric ozone monitoring: GOMOS on Envisat, Earth observation quarterly, 17–20, 2000. 11113

Bertaux, J. L., Megie, G., Widemann, T., Chassefière, E., Pellinen, R., Kyrölä, E., Korpela, S., and Simon, P.: Monitoring of ozone trend by stellar occultations: The GOMOS instrument, Adv. Space Res., 11, 3237–3242, 1991. 11113

Bertaux, J. L., Kyrölä, E., Fussen, D., Hauchecorne, A., Dalaudier, F., Sofieva, V., Tamminen, J., Vanhellemont, F., Fanton d'Andon, O., Barrot, G., Mangin, A., Blanot, L., Lebrun, J. C., Pérot, K., Fehr, T., Saavedra, L., and Fraisse, R.: Global ozone monitoring by occultation of stars: an overview of GOMOS measurements on ENVISAT, Atmos. Chem. Phys. Discuss.,

10, 9917–10076, 2010, http://www.atmos-chem-phys-discuss.net/10/9917/2010/. 11113, 11116
Carn, S. A., Krotkov, N. A., Yang, K., Hoff, R. M., Prata, A. J., Krueger, A. J., Loughlin, S. C., and Levelt, P. F.: Extended observations of volcanic $SO_2$ and sulfate aerosol in the stratosphere, Atmos. Chem. Phys. Discuss., 7, 2857–2871, 2007, http://www.atmos-chem-phys-discuss.net/7/2857/2007/. 11121
Chin, M. and Davis, D. D.: A reanalysis of carbonyl sulfide as a source of stratospheric background sulfur aerosol, J. Geophys. Res., 100, 8993–9005, 1995. 11111
Chu, W., McCormick, M., Lenoble, J., Brogniez, C., and Pruvost, P.: SAGE II inversion algorithm, J. Geophys. Res., 94, 8339–8351, 1989. 11118
Crutzen, P.: The possible importance of OCS for the sulfate layer of the stratosphere, Geophys. Res. Lett., 3, 73–76, 1976. 11111
Deshler, T., Hervig, M. E., Hofmann, D. J., Rosen, J. M., and Liley, J. B.: Thirty years of in situ stratospheric aerosol size distribution measurements from Laramie, Wyoming (41N), using balloon-borne instruments, J. Geophys. Res., 108(D5), 4167, doi:10.1029/2002JD002514, 2003. 11111
Deshler, T., Anderson-Sprecher, R., Jäger, H., Barnes, J., Hofmann, D. J., Clemesha, B., Simonich, D., Osborn, M., Grainger, R. G., and Godin-Beeckmann, S.: Trends in the nonvolcanic component of stratospheric aerosol over the period 1971–2004, J. Geophys. Res., 111, D01201, doi:10.1029/2005JD006089, 2006. 11111
Hofmann, D., Barnes, J., O'Neill, M., Trudeau, M., and Neely, R.: Increase in background stratospheric aerosol observed with lidar at Mauna Loa Observatory and Boulder, Colorado, Geophys. Res. Lett., 36, L15808, doi:10.1029/2009GL039008, 2009. 11111, 11122
Jensen, E. J., Toon, O. B., Selkirk, H. B., Spinhirne, J. D., and Schoeberl, M. R.: On the formation and persistence of subvisible cirrus clouds near the tropical tropopause, J. Geophys. Res., 101, 21361–21375, 1996. 11112, 11118
Junge, C., Chagnon, C., and Manson, J.: Stratospheric aerosols, J. Meteorol., 18, 80–108, 1961. 11111
Kamei, A., Sugimoto, N., Matsui, I., Shimizu, A., and Shibata, T.: Volcanic aerosol layer observed by shipboard lidar over the tropical western Pacific, Scientific Online Letters on the Atmosphere, 2, 001–004, doi:10.2151/sola.2006-001, 2006. 11121
Kyrölä, E., Tamminen, J., Leppelmeier, G., Sofieva, V., Hassinen, S., Bertaux, J., Hauchecorne, A., Dalaudier, F., Cot, C., Korablev, O., Fanton d'Andon, O., Barrot, G., Mangin, A., Theodore,

B., Guirlet, M., Etanchaud, F., Snoeij, P., Koopman, R., Saavedra, L., Fraisse, R., Fussen, D., and Vanhellemont, F.: GOMOS on Envisat – an overview, Adv. Space Res., 33, 1020–1028, 2004. 11113

Kyrölä, E., Tamminen, J., Sofieva, V., Bertaux, J. L., Hauchecorne, A., Dalaudier, F., Fussen, D., Vanhellemont, F., Fanton d'Andon, O., Barrot, G., Guirlet, M., Mangin, A., Blanot, L., Fehr, T., Saavedra de Miguel, L., and Fraisse, R.: Retrieval of atmospheric parameters from GOMOS data, Atmos. Chem. Phys. Discuss., 10, 10145–10217, 2010, http://www.atmos-chem-phys-discuss.net/10/10145/2010/. 11115, 11116

Leung, F.-Y. T., Colussi, A. J., Hoffmann, M. R., and Toon, G. C.: Isotopic fractionation of carbonyl sulfide in the atmosphere: Implications for the source of background stratospheric sulfate aerosol, Geophys. Res. Lett., 29(10), 1474, doi:10.1029/2001GL013955, 2002. 11111

Lucke, R. L., Korwan, D. R., Bevilacqua, R., Hornstein, J. S., Shettle, E. P., Chen, D. T., Daehler, M., Lumpe, J. D., Fromm, M. D., Debrestian, D., Neff, B., Squire, M., König-Langlo, G., and Davies, J.: The Polar Ozone and Aerosol Measurement (POAM) III instrument and early validation results, J. Geophys. Res., 104, 18785–18799, 1999. 11118

Poole, L. R. and McCormick, M. P.: Airborne lidar observations of Arctic polar stratospheric clouds: Indications of two distinct growth stages, Geophys. Res. Lett., 15, 21–23, 1988. 11111

Poole, L. R., Trepte, C. R., Harvey, V. L., Toon, G. C., and Van Valkenburg, R. L.: SAGE III observations of Arctic polar stratospheric clouds – December 2002, Geophys. Res. Lett., 30(23), 2216, doi:10.1029/2003GL018496, 2003. 11123

Prata, A. J., Carn, S. A., Stohl, A., and Kerkmann, J.: Long range transport and fate of a stratospheric volcanic cloud from Soufrière Hills volcano, Montserrat, Atmos. Chem. Phys., 7, 5093–5103, 2007, http://www.atmos-chem-phys.net/7/5093/2007/. 11121

Robock, A.: Volcanic eruptions and climate, Rev. Geophys., 38, 191–219, 2000. 11111

Rodgers, C.: Inverse Methods for Atmospheric Sounding – Theory and Practice, World Scientific, first edn., 2000. 11115

Smithsonian Institution: Bulletin of the Global Volcanism Network, 30(2): February 2005, Manam, online available at: http://www.volcano.si.edu/reports/bulletin, (last access: April 2010) 2005. 11121

Sofieva, V. F., Kan, V., Dalaudier, F., Kyrölä, E., Tamminen, J., Bertaux, J.-L., Hauchecorne, A., Fussen, D., and Vanhellemont, F.: Influence of scintillation on quality of ozone monitoring by

GOMOS, Atmos. Chem. Phys., 9, 9197–9207, 2009, http://www.atmos-chem-phys.net/9/9197/2009/. 11115
Solomon, S., Borrmann, S., Garcia, R. R., Portmann, R., Thomason, L., Poole, L. R., Winker, D., and McCormick, M. P.: Heterogeneous chlorine chemistry in the tropopause region, J. Geophys. Res., 102, 21411–21429, 1997. 11112
Strawa, A. W., Drdla, K., Fromm, M., Pueschel, R. F., Hoppel, K. W., Browell, E. V., Hamill, P., and Dempsey, D. P.: Discriminating Types Ia and Ib polar stratospheric clouds in POAM satellite data, J. Geophys. Res., 107(D20), 8291, doi:10.1029/2001JD000458, 2002. 11123
Thomason, L. W., Pitts, M. C., and Winker, D. M.: CALIPSO observations of stratospheric aerosols: a preliminary assessment, Atmos. Chem. Phys., 7, 5283–5290, 2007, http://www.atmos-chem-phys.net/7/5283/2007/. 11122
Thomason, L. W. and Taha, G.: SAGE III aerosol extinction measurements: Initial results, Geophys. Res. Lett., 30(12), 1631, doi:10.1029/2003GL017317, 2003. 11118
Twomey, S.: Introduction to the Mathematics of Inversion in Remote Sensing and Indirect Measurements, Elsevier Scientific Publishing Company, New York, USA, 1985. 11115
Vanhellemont, F., Fussen, D., Bingen, C., Kyrölä, E., Tamminen, J., Sofieva, V., Hassinen, S., Verronen, P., Seppälä, A., Bertaux, J. L., Hauchecorne, A., Dalaudier, F., Fanton d'Andon, O., Barrot, G., Mangin, A., Theodore, B., Guirlet, M., Renard, J. B., Fraisse, R., Snoeij, P., Koopman, R., and Saavedra, L.: A 2003 stratospheric aerosol extinction and PSC climatology from GOMOS measurements on Envisat, Atmos. Chem. Phys., 5, 2413–2417, 2005, http://www.atmos-chem-phys.net/5/2413/2005/. 11113, 11124
Vanhellemont, F., Fussen, D., Dodion, J., Bingen, C., and Mateshvili, N.: Choosing a suitable analytical model for aerosol extinction spectra in the retrieval of UV/visible satellite occultation measurements, J. Geophys. Res., 111, D23203, doi:10.1029/2005JD006941, 2006. 11114
Vanhellemont, F., Tetard, C., Bourassa, A., Fromm, M., Dodion, J., Fussen, D., Brogniez, C., Degenstein, D., Gilbert, K. L., Turnbull, D. N., Bernath, P., Boone, C., and Walker, K. A.: Aerosol extinction profiles at 525 nm and 1020 nm derived from ACE imager data: comparisons with GOMOS, SAGE II, SAGE III, POAM III, and OSIRIS, Atmos. Chem. Phys., 8, 2027–2037, 2008, http://www.atmos-chem-phys.net/8/2027/2008/. 11118
Wang, P., Minnis, P., McCormick, M., Kent, G., and Skeens, K.: A 6-year climatology of cloud occurrence frequency from Stratospheric Aerosol and Gas Experiment II observations (1985–1990), J. Geophys. Res., 101, 29407–29429, 1996. 11112

**Table 1.** GOMOS aerosol extinction retrievals: comparison data set; coincidence window: (500 km, 1/2 day).

| Instrument | Version | Wavelength | # of coincidences | Time period considered |
|---|---|---|---|---|
| SAGE II | 6.20 | 525 nm | 6227 | 27 August 2002–5 March 2005 |
| SAGE III | 3.00 | 596 nm | 6258 | 7 November 2002–3 December 2005 |
| POAM III | 4.00 | 603 nm | 11641 | 26 August 2002–3 December 2005 |

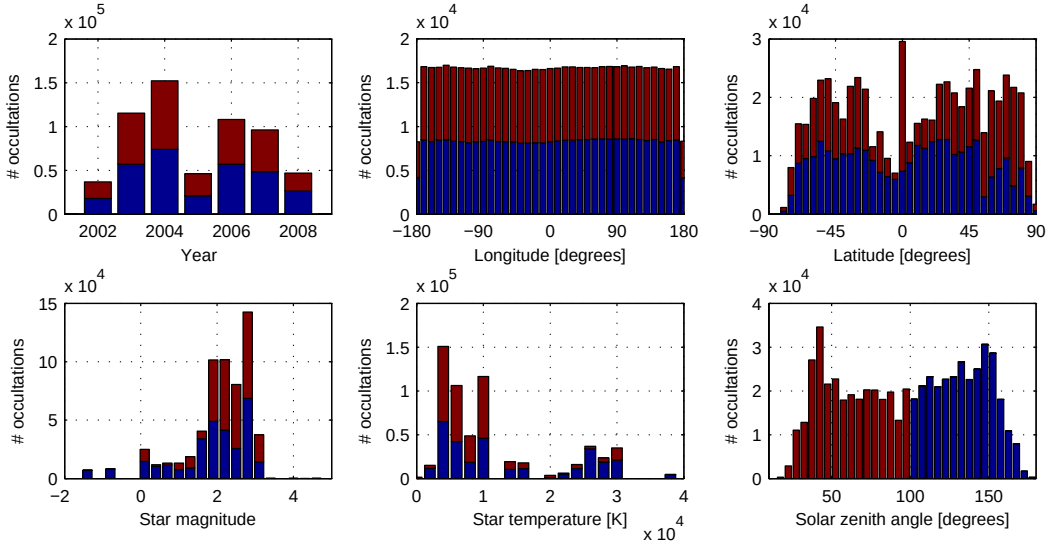


**Fig. 1.** Occultation statistics for the entire GOMOS data set spanning the period August 2002–May 2008. Shown are histograms representing the number of GOMOS occultations as function of (from left to right, top to bottom) year, longitude, latitude, star magnitude, star temperature and solar zenith angle. Blue histograms refer to the fraction of occultations in dark limb, red ones to the fraction in bright limb.



ACPD
10, 11109–11138, 2010

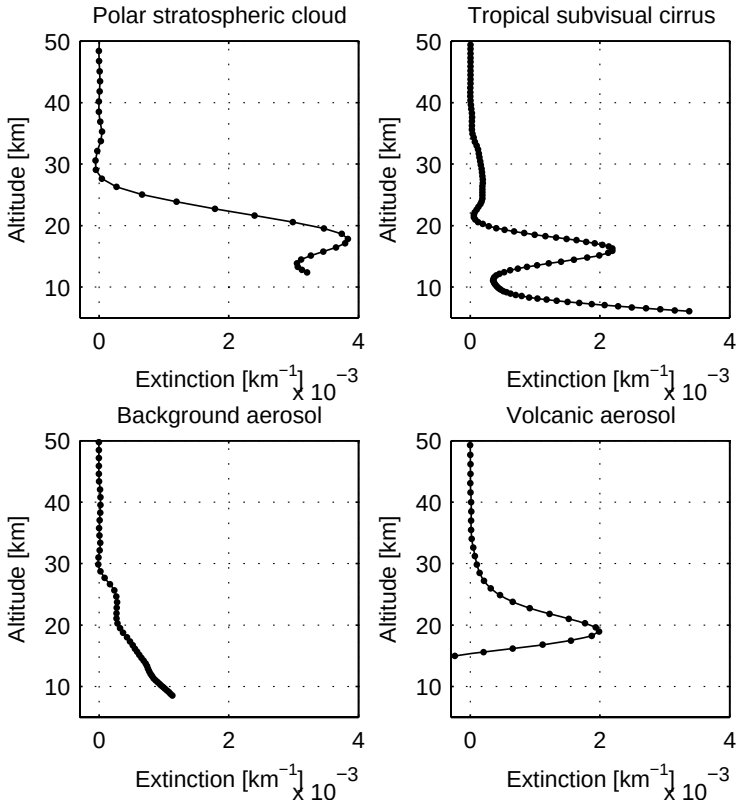


**Fig. 2.** Individual GOMOS particle extinction profiles: a Polar Stratospheric Cloud (30 July 2003, 72.57° S, 2.18° W), a tropical subvisual cirrus cloud (7 October 2002, 0.52° S, 78.69° E), background stratospheric aerosols (12 September 2003, 43.34° S, 137.36° W), volcanic stratospheric aerosols (9 January 2007, 4.52° S, 27.15° E). All plots have the same scale, in order to facilitate comparisons of magnitude.



ACPD
10, 11109–11138, 2010

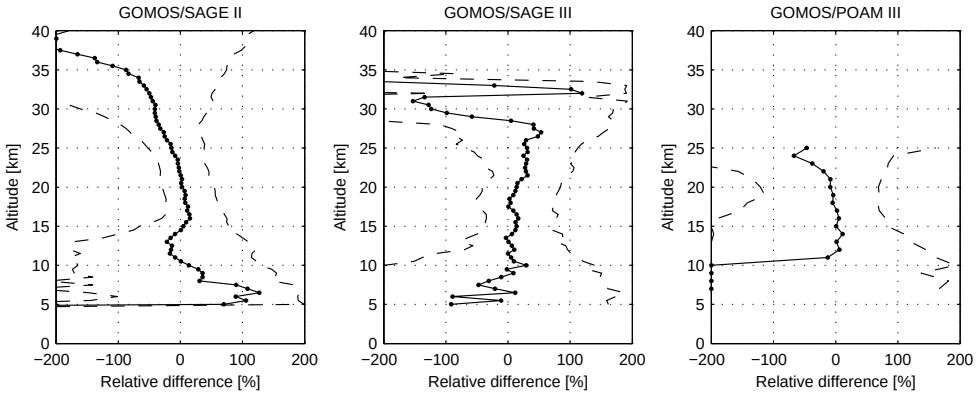


**Fig. 3.** Comparison of GOMOS aerosol extinction profiles with other satellite measurements: SAGE II at 525 nm (left panel), SAGE III at 596 nm (middle panel) and POAM III at 603 nm (right panel). Shown are the statistics for the relative differences, calculated as $100 \times 2(p_{\mathrm{GOMOS}} - p_{\mathrm{SAT}})/|p_{\mathrm{GOMOS}} + p_{\mathrm{SAT}}|$. The median of the set of relative differences is shown with full lines and dots. Dashed lines indicate the spread, given by the 16th and 84th percentile.



ACPD
10, 11109–11138, 2010

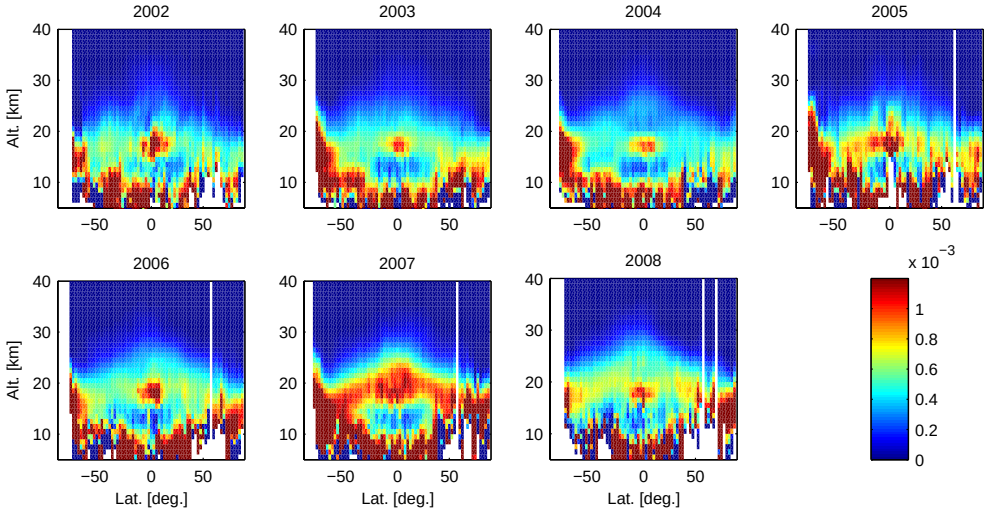


**Fig. 4.** Yearly zonal median values of (dark limb) aerosol extinction at 500 nm for the entire GOMOS mission. All features that are to be expected are present: the stratospheric aerosol layer, PSCs in the Antarctic region, tropical subvisual cirrus clouds. Notice the enhanced stratospheric aerosol layer in 2007, resulting from the Soufrière Hills eruption in May 2006. Years that are sampled incompletely: 2002 (start of the data set: August 2002), 2005 (instrument failure) and 2008 (end of available data set).



ACPD
10, 11109–11138, 2010

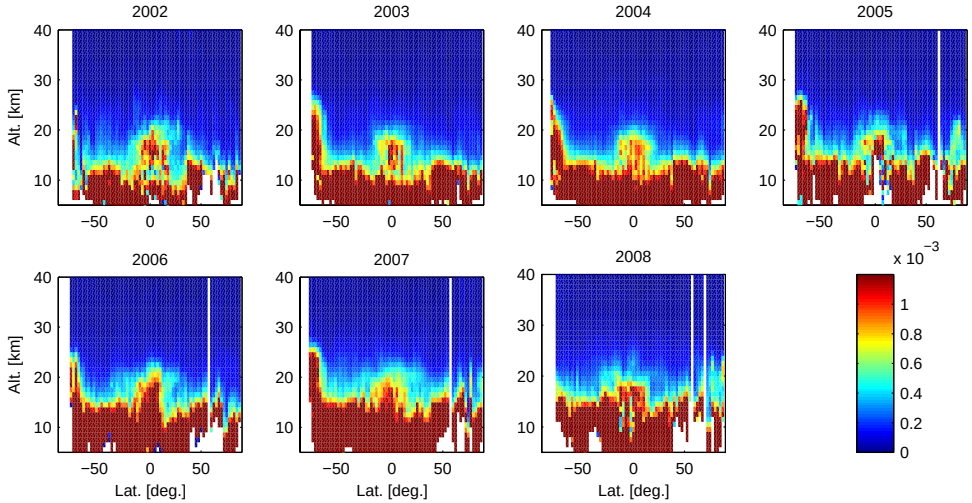


**Fig. 5.** Yearly zonal variability of (dark limb) aerosol extinction at 500 nm for the entire GOMOS mission. Variability is calculated as half the difference of the 84th and 16th percentile, and is determined by measurement error and (more importantly) by natural aerosol/cloud variability. "On/off" events such as clouds (tropical cirrus, Antarctic PSCs) of course exhibit large variability, while slowly changing features (backgrounds aerosol layer) vary little. Years that are sampled incompletely: 2002 (start of the data set: august 2002), 2005 (instrument failure) and 2008 (end of available data set).



ACPD
10, 11109–11138, 2010



CC BY

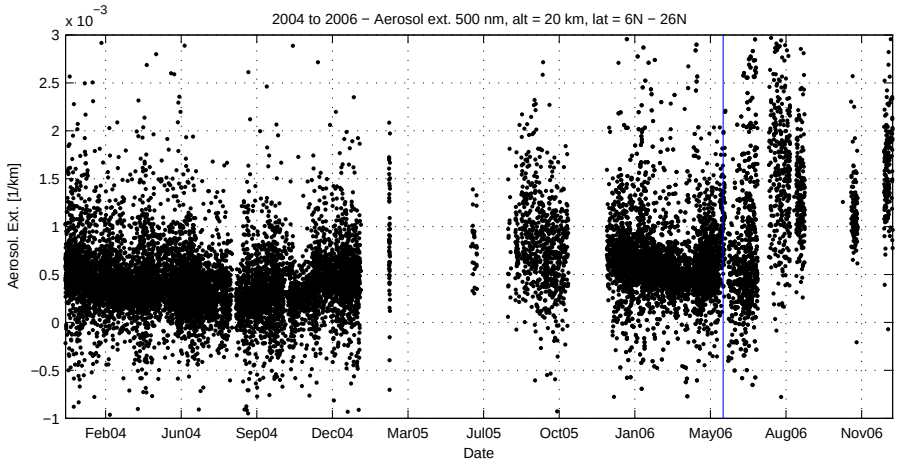


**Fig. 6.** A 2004–2006 GOMOS aerosol extinction time series at an altitude of 20 km. All data within a latitude band from 6° N–26° N are shown. Clearly visible are the background aerosol condition in 2004, the possible declining tail of the post-eruptive aerosols resulting from the Manam volcano (Papua New Guinea, 27–28 January 2005; first vertical line), and the enhanced aerosol levels following the eruption of Soufrière Hills (Montserrat, 20 May 2006, second vertical line).



ACPD
10, 11109–11138, 2010

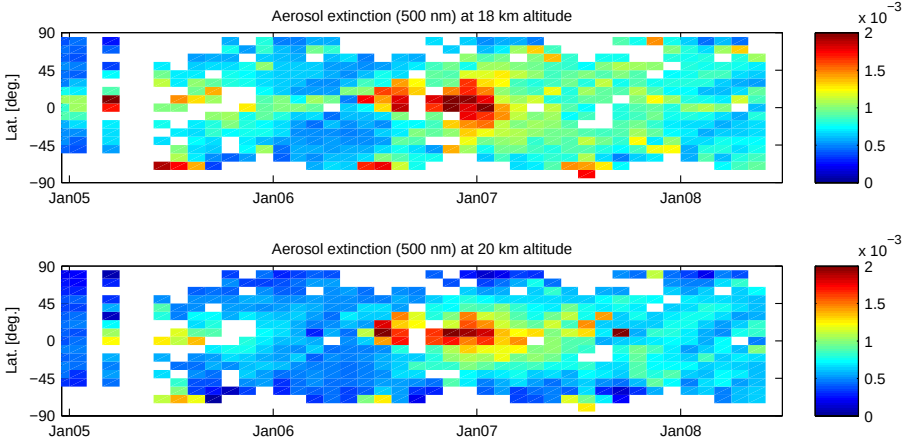


**Fig. 7.** Checkerboard plots showing the median of binned 500 nm aerosol extinction data as function of latitude and time, at an altitude of 18 km (upper panel) and 20 km (lower panel). Notice the elevated values after early 2005, and after the end of May 2006. The global spreading is clearly visible in the latter case.



ACPD
10, 11109–11138, 2010

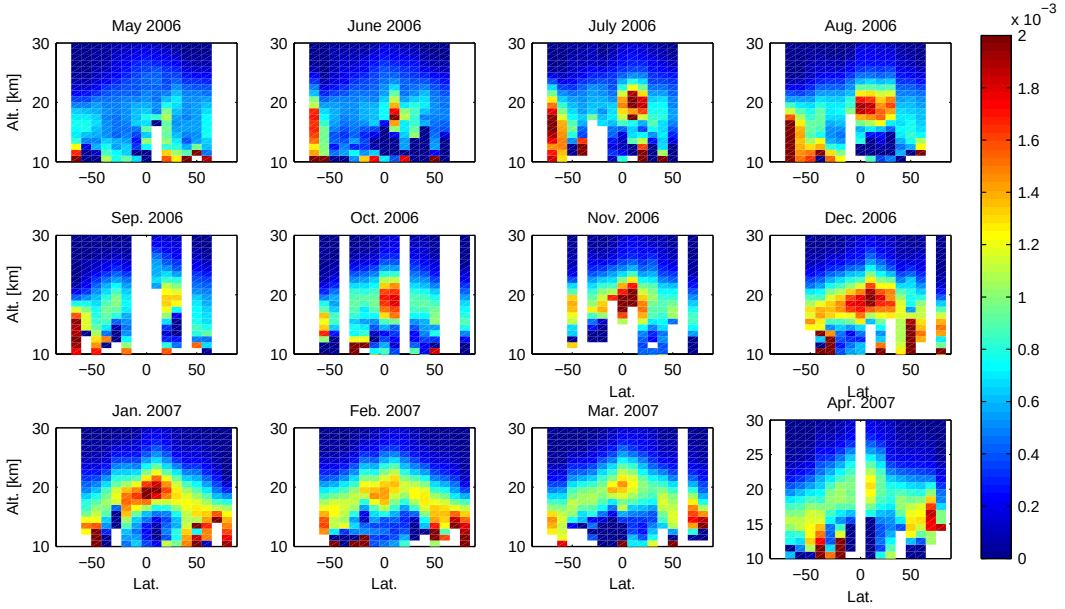


**Fig. 8.** Evolution of the volcanic stratospheric aerosols resulting from the Soufrière Hills eruption on 20 May 2006. Shown are monthly zonal median aerosol extinction coefficients at 500 nm. Starting from the eruption site (Montserrat, 16.72° N, 62.18° W), the plume disperses poleward and encircles the entire earth within a year.



ACPD
10, 11109–11138, 2010

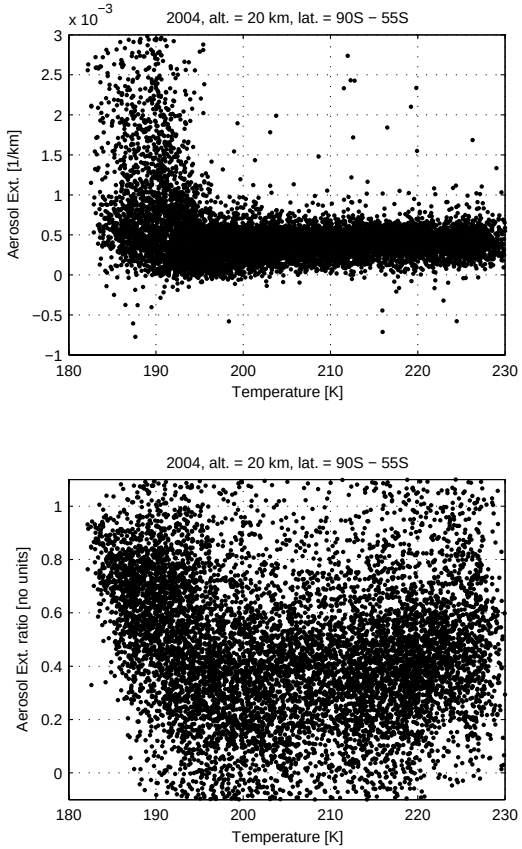


**Fig. 9.** GOMOS measurements of Polar Stratospheric Clouds. Top panel: optical extinction at 500 nm versus temperature at an altitude of 20 km, for all dark limb occultations in 2004 at latitudes below 55° S. Bottom panel: extinction ratio (600/400 nm), derived from the same measurements.



ACPD
10, 11109–11138, 2010